

tCURLoRA: Tensor CUR Decomposition Based Low-Rank Parameter Adaptation and Its Application in Medical Image Segmentation

Guanghua He^{1,2}, Wangang Cheng², Hancan Zhu², Xiaohao Cai³, and Gaohang Yu^{1*}

¹ Department of Mathematics, Hangzhou Dianzi University, Hangzhou, 310018, China

² School of Mathematics, Physics and Information, Shaoxing University, Shaoxing, 312000, China

³ School of Electronics and Computer Science, University of Southampton, Southampton, SO17
1BJ, UK

* Corresponding author: Gaohang Yu, E-mail address: maghyu@163.com

Abstract

Transfer learning, by leveraging knowledge from pre-trained models, has significantly enhanced the performance of target tasks. However, as deep neural networks scale up, full fine-tuning introduces substantial computational and storage challenges in resource-constrained environments, limiting its widespread adoption. To address this, parameter-efficient fine-tuning (PEFT) methods have been developed to reduce computational complexity and storage requirements by minimizing the number of updated parameters. While matrix decomposition-based PEFT methods, such as LoRA, show promise, they struggle to fully capture the high-dimensional structural characteristics of model weights. In contrast, high-dimensional tensors offer a more natural representation of neural network weights, allowing for a more comprehensive capture of higher-order features and multi-dimensional interactions. In this paper, we propose tCURLoRA, a novel fine-tuning method based on tensor CUR decomposition. By concatenating pre-trained weight matrices into a three-dimensional tensor and applying tensor CUR decomposition, we update only the lower-order tensor components during fine-tuning, effectively reducing computational and storage overhead. Experimental results demonstrate that tCURLoRA outperforms existing PEFT methods in medical image segmentation tasks.

Keywords: Parameter-efficient fine-tuning, tensor CUR decomposition, deep learning, transfer learning, medical image segmentation

1. Introduction

Transfer learning, a key research area in deep learning, has significantly enhanced the performance of target tasks, particularly in data-scarce scenarios, by transferring knowledge from pre-trained models [1, 2]. However, as the scale of deep learning models continues to expand, full fine-tuning presents significant computational and storage challenges in resource-constrained environments, limiting its practical applicability. To address this issue, parameter-efficient fine-tuning (PEFT) methods have been developed. By either limiting the range of parameters updated or reducing the number of parameters that require updating in deep neural networks (DNNs), PEFT methods effectively reduce both computational complexity and storage requirements, making them a prominent research focus in recent years [3-5].

Low-Rank Adaptation (LoRA) is a well-established method within PEFT that reduces the number of trainable parameters by using low-rank matrices for incremental updates to pre-trained weights in DNNs, while maintaining high model performance [5]. To further improve the model's generalization,

Hydra introduces a multi-head low-rank adaptation approach that combines parallel and sequential branching structures, thereby enhancing the model’s expressive capacity [6]. PiSSA, based on singular value decomposition (SVD), boosts fine-tuning efficiency by leveraging the primary singular values and their corresponding vectors [7]. CURLoRA incorporates CUR matrix decomposition to address catastrophic forgetting, enabling continuous learning while maintaining high performance [8]. More recently, PMSS utilizes CUR matrix decomposition to improve model adaptability in complex tasks by selecting skeletal substructures from the pre-trained weight matrix [9].

Current PEFT methods based on low-rank adaptation predominantly rely on matrix decomposition. However, these approaches often fail to fully capture the high-dimensional structural characteristics of deep neural network weights. High-dimensional tensors, in contrast, provide a more natural representation, enabling the capture of higher-order features and multi-dimensional interactions, thereby offering superior expressive power [10]. Integrating tensor decomposition into PEFT could not only enhance transfer learning efficiency but also uncover latent features within high-dimensional weight representations. In this paper, we propose a key substructure fine-tuning method based on tensor CUR decomposition, called tCURLoRA. Specifically, we first concatenate the pre-trained weight matrices along the frontal dimension to construct a three-dimensional tensor representation, which is then decomposed using tensor CUR decomposition. During the fine-tuning process, only the lower-order tensor components are updated, effectively reducing the number of trainable parameters and minimizing computational and storage overhead. The main contributions of this work are summarized as follows:

- **Novel integration of tensor CUR decomposition:** By extracting key substructures from the tensor and selectively fine-tuning the associated parameters, we improve fine-tuning efficiency by focusing on the most significant components.
- **Reduction of computational complexity and memory usage:** The proposed tCURLoRA method optimizes the decomposition of parameters, significantly lowering both computational load and storage demands, thus enhancing overall resource efficiency.
- **Improved performance in medical image segmentation:** Experimental results show that applying the tCURLoRA method to transfer learning in medical image segmentation tasks leads to significant performance improvement over existing PEFT approaches.

2. Related work

2.1 Deep Neural Networks

DNNs have evolved from simple architectures into highly complex models, with their applications expanding as computational power and data availability have advanced. LeNet [11], one of the earliest DNN models, introduced convolutional and pooling layers for handwritten digit recognition, establishing the foundation for the development of convolutional neural networks (CNNs). Building on this, AlexNet [12] demonstrated the immense potential of DNNs in large-scale image classification tasks. By employing a deeper network architecture and the ReLU activation function, it marked a milestone achievement in the field of deep learning. VGG [13] further advanced DNNs by increasing depth through the simple stacking of convolutional layers, pioneering the trend toward more complex architectures. ResNet [14] addressed critical challenges in very deep networks, such as vanishing gradients and performance degradation, through the introduction of residual learning, marking a milestone in the evolution of DNNs. More recently, the Transformer model [15] has challenged the dominance of CNNs in computer vision by introducing the self-attention mechanism, providing novel insights and solutions

for image processing tasks.

Image segmentation, a fundamental task in computer vision, has emerged as a pivotal application of deep learning techniques. For example, fully convolutional networks [16] were the first end-to-end networks specifically designed for image segmentation, enabling pixel-wise predictions through fully convolutional operations. Subsequently, U-Net [17] introduced an encoder-decoder architecture specifically designed for medical image segmentation. By incorporating skip connections to preserve high-resolution features, it significantly improved performance in small object segmentation tasks. DeepLab [18] further advanced semantic segmentation by introducing dilated convolutions and conditional random fields, improving boundary refinement and multi-scale feature fusion, thus establishing itself as a benchmark model in the field. Mask R-CNN [19] combined semantic segmentation with object detection, facilitating the progression of instance segmentation. Boundary-Aware Networks [20] improved instance segmentation by enhancing the model's ability to identify and accurately delineate complex boundary regions. In recent years, Transformer-based models, such as vision Transformer (ViT) [21], have gained prominence in computer vision. By leveraging large-scale parameters, ViT has significantly enhanced segmentation accuracy, setting new performance benchmarks and advancing the state of the field.

2.2 Tensor Decomposition Methods

Tensor decomposition is a powerful tool for analyzing multi-dimensional data. By representing high-dimensional tensors in lower-dimensional forms, it uncovers the underlying structures within the data, making it highly applicable in fields such as signal processing, machine learning, and medical image analysis [22, 23]. Several tensor decomposition methods have been proposed, including CANDECOMP/PARAFAC (CP) decomposition [24, 25], Tucker decomposition [26], Tensor Train (TT) decomposition [27], and Tensor CUR decomposition [28, 29]. CP decomposition is one of the fundamental tensor decomposition methods, factorizing a tensor into a sum of rank-one tensors to uncover latent patterns within the data. Despite its structural simplicity, CP decomposition is highly sensitive to the choice of decomposition rank and often poses optimization challenges in practical applications [30]. Tucker decomposition captures multi-dimensional relationships through a core tensor and factor matrices, with applications in image compression, video analysis, and multi-dimensional statistical modeling. Compared to CP decomposition, it is more expressive but computationally intensive. Recent optimizations have improved its efficiency, especially for large-scale image processing [31, 32]. TT decomposition breaks down high-dimensional tensors into a series of smaller three-dimensional tensors, optimizing storage and computational efficiency [33]. Finally, Tensor CUR decomposition, an extension of matrix CUR decomposition, performs low-rank approximation by selecting tensor rows, columns, and fibers. This approach reduces computational and storage complexity and has been widely applied in recommendation systems, sensor networks, and medical imaging [34].

In recent years, tensor decomposition has become a prominent research focus in deep learning [35]. Initially, it was widely applied to network compression and acceleration, with techniques such as decomposing convolutional kernels and fully connected layer parameters significantly reducing the storage and computational costs of deep learning models [36, 37]. For example, TT decomposition has been used to reduce the number of parameters in fully connected layers, enabling the efficient deployment of deep learning models on resource-constrained devices [38]. Additionally, Tucker decomposition and tensor ring decomposition have been increasingly applied in multimodal learning, facilitating effective feature fusion across diverse modalities, such as images, text, and audio [39]. In medical image diagnosis,

for instance, combining CT and MRI data through tensor decomposition has significantly improved disease prediction accuracy [40]. Tensor decomposition also plays a pivotal role in optimizing attention mechanisms. For example, low-rank decomposition techniques have been utilized to optimize the multi-head attention mechanism in Transformer models, reducing computational complexity [41]. Moreover, tensorized weight training and low-precision computation leverage tensor decomposition to enhance weight storage efficiency and accelerate computations, enabling the deployment of DNNs on resource-constrained embedded systems [42]. These applications highlight the broad potential and innovative capabilities of tensor decomposition in advancing deep learning technologies.

2.3 Parameter-Efficient Fine-Tuning Methods

Unlike traditional transfer learning methods, PEFT approaches significantly reduce the reliance on large labeled datasets and extensive computational resources by adjusting only a small subset of parameters in pre-trained models [3-5]. For instance, Hu et al. proposed the LoRA method, which applies low-rank matrix decomposition to the weight matrices of pre-trained models, enabling model adaptation without modifying the underlying architecture [5]. Building on this, Chen et al. proposed SuperLoRA, which optimizes parameter adaptation in multi-layer attention modules, enhancing model performance while maintaining parameter efficiency [43]. Liu et al. developed the Dora method, combining weight decomposition with low-rank adaptation to optimize storage and computational efficiency in deep learning models [44]. Meng et al. introduced PISSA, which adapts the primary singular values and corresponding vectors in large language models, enabling efficient fine-tuning [7]. Fawi et al. presented CURLoRA, integrating CUR matrix decomposition to mitigate catastrophic forgetting, thus enhancing continuous learning capabilities [8]. Moreover, Wang et al. proposed PMSS, utilizing CUR matrix decomposition to extract skeletal substructures from pre-trained weight matrices, improving the model’s ability to perform high-rank updates in complex tasks [9].

Recently, tensor decomposition methods have been increasingly incorporated into PEFT. Although this area is still under active exploration, several studies have highlighted its preliminary value. For instance, Bershtsky et al. proposed the LoTR technique, which applies tensor Tucker decomposition for low-rank adaptation, optimizing model weights, reducing parameters, and improving computational efficiency [45]. Jie and Deng’s Fact method combines tensor TT and Tucker decomposition, specifically tailored for visual Transformer models. By selectively adjusting key factors, this approach enhances model performance in specific visual tasks [46]. Si et al. proposed FLoRA, which utilizes Tucker decomposition to apply low-rank adjustments to high-dimensional parameter spaces while preserving the structure’s topological consistency [47]. Additionally, He et al. introduced a T-SVD decomposition approach, decomposing pre-trained parameter tensors into primary and residual components, updating only the primary tensor during fine-tuning [48]. These studies suggest that, although the application of tensor decomposition in PEFT is still evolving, these methods hold significant potential for reducing computational and storage overhead while improving model optimization.

3. Method

Transformer-based neural networks typically stack identical Transformer structures multiple times, resulting in parameter matrices of uniform size. Currently, most low-rank decomposition-based PEFT methods independently fine-tune each parameter matrix. Figure 1(a) illustrates a PEFT method based on matrix CUR decomposition [8, 9]. As shown, this method independently applies matrix CUR decomposition to fine-tune each weight matrix. Specifically, let $\tilde{W}_i \in R^{n_1 \times n_2}, i = 1, 2, \dots, n_3$ represent

the n_3 pre-trained weight matrices. During fine-tuning, we keep these pre-trained weights fixed while updating their increments $\Delta W_i, i = 1, 2, \dots, n_3$. The parameter update process is expressed as:

$$W_i = \tilde{W}_i + \Delta W_i, i = 1, 2, \dots, n_3. \quad (1)$$

Using matrix CUR decomposition, ΔW_i is expressed as:

$$\Delta W_i = C_i U_i R_i, i = 1, 2, \dots, n_3,$$

where $C_i \in R^{n_1 \times c}$ contains c ($c \ll n_2$) columns sampled from \tilde{W}_i , and $R_i \in R^{r \times n_2}$ contains r ($r \ll n_1$) rows sampled from \tilde{W}_i . Both C_i and R_i remain fixed during fine-tuning, while $U_i \in R^{c \times r}$ is typically initialized to zero and updated during the fine-tuning process. Here, c and r represent the numbers of sampled columns and rows, respectively. To reduce the number of hyperparameters, c and r are typically set to be equal [8, 9].

As shown in Figure 1(b), to fully leverage the properties of high-dimensional data, we propose a PEFT method based on tensor CUR decomposition, referred to as tCURLoRA. Specifically, the pre-trained parameter matrices are concatenated along the frontal dimension to form a three-dimensional tensor $\tilde{\mathcal{W}}$. Fine-tuning is performed using tensor CUR decomposition, expressed as:

$$\mathcal{W} = \tilde{\mathcal{W}} + \Delta \mathcal{W} = \tilde{\mathcal{W}} + \mathcal{C} * \mathcal{U} * \mathcal{R}, \quad (2)$$

where $\tilde{\mathcal{W}} \in R^{n_1 \times n_2 \times n_3}$ remains unchanged during fine-tuning; $\mathcal{C} \in R^{n_1 \times r \times n_3}$ and $\mathcal{R} \in R^{r \times n_2 \times n_3}$ are low-rank tensors derived from the tensor CUR decomposition of $\tilde{\mathcal{W}}$, and they also remain fixed. $\mathcal{U} \in R^{r \times r \times n_3}$ is initialized as a zero tensor and updated during fine-tuning. Here, r denotes the number of sampled columns and rows. The operator "*" represents the tensor product.

The following sections provide an overview of key concepts and methods: Section 2.1 introduces the tensor product, Section 2.2 discusses tensor CUR decomposition, and Section 2.3 presents tCURLoRA for fine-tuning UNETR parameters [49], as an example.

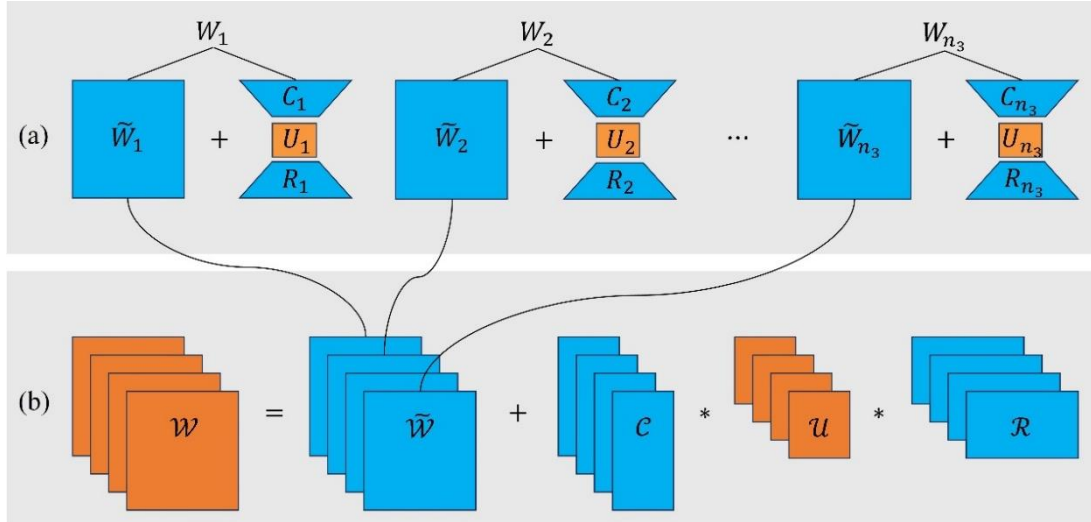


Figure 1. Comparison of PEFT Methods: Matrix CUR Decomposition vs. Tensor CUR Decomposition. (a) Fine-tuning weight matrices independently with matrix CURLoRA. (b) Concatenating weight matrices into a three-dimensional tensor for fine-tuning with tCURLoRA. In the figure, blue indicates frozen parameters, orange indicates updated parameters, and * represents the tensor product.

2.1 Tensor Product

The tensor product is defined as follows [23].

Definition 1. Let $\mathcal{A} \in R^{n_1 \times n_2 \times n_3}$ and $\mathcal{B} \in R^{n_2 \times l \times n_3}$ be two third-order tensors. The t-product $\mathcal{A} * \mathcal{B}$ is a tensor of size $n_1 \times l \times n_3$, defined as:

$$\mathcal{A} * \mathcal{B} = \text{fold}(\text{circ}(\mathcal{A})\text{MatVec}(\mathcal{B})),$$

with operations circ , MatVec , and fold given below.

The $\text{circ}(\mathcal{A})$ is constructed by arranging the frontal slices of tensor \mathcal{A} into a block-circulant matrix. The corresponding expression for $\text{circ}(\mathcal{A})$ is given by:

$$\text{circ}(\mathcal{A}) = \begin{bmatrix} A_1 & A_{n_3} & \cdots & A_2 \\ A_2 & A_1 & \cdots & A_3 \\ \vdots & \vdots & \ddots & \vdots \\ A_{n_3} & A_{n_3-1} & \cdots & A_1 \end{bmatrix},$$

where $A_i = \mathcal{A}(:, :, i)$ for $i = 1, 2, \dots, n_3$ represents the i th frontal slice of tensor \mathcal{A} . The operation $\text{MatVec}(\mathcal{B})$ vertically stacks the two-dimensional slices of tensor \mathcal{B} into a matrix, which is expressed as:

$$\text{MatVec}(\mathcal{B}) = \begin{bmatrix} B_1 \\ B_2 \\ \vdots \\ B_{n_3} \end{bmatrix},$$

where $B_i = \mathcal{B}(:, :, i)$ for $i = 1, 2, \dots, n_3$ is the i th frontal slice of tensor \mathcal{B} . The operation "fold" restores the matrix $\text{MatVec}(\mathcal{B})$ back to tensor \mathcal{B} , i.e., $\text{fold}(\text{MatVec}(\mathcal{B})) = \mathcal{B}$.

We know that a circulant matrix can be block-diagonalized using the Discrete Fourier Transform (DFT), i.e., $(F \otimes I_{n_1})\text{circ}(\mathcal{A})(F^* \otimes I_{n_2})$ is a block-diagonal matrix [50]; therefore, we have:

$$\text{circ}(\mathcal{A})\text{MatVec}(\mathcal{B}) = (F^* \otimes I_{n_1})((F \otimes I_{n_1})\text{circ}(\mathcal{A})(F^* \otimes I_{n_2}))(F \otimes I_{n_2})\text{MatVec}(\mathcal{B}),$$

where $F \in R^{n_3 \times n_3}$ is the DFT matrix, F^* is the conjugate transpose of F , \otimes denotes the Kronecker product, and I_{n_1} is the identity matrix of size $n_1 \times n_1$. Thus, to compute $\mathcal{A} * \mathcal{B}$, we follow these steps: i) apply the DFT to tensors \mathcal{A} and \mathcal{B} along their third dimension, converting them into the frequency domain; ii) perform matrix multiplication on the corresponding two-dimensional slices of the transformed tensors; and iii) apply the inverse DFT along the third dimension of the resulting tensor to return it to the time domain, yielding the final result.

2.2 Tensor CUR Decomposition

The tensors \mathcal{C} and \mathcal{R} introduced in Equation (2) are obtained through the tensor CUR decomposition of $\tilde{\mathcal{W}}$. We adopt the tensor CUR decomposition method from [29]. Specifically, we first apply the Fast Fourier Transform (FFT) along the third dimension to the tensor $\tilde{\mathcal{W}} \in R^{n_1 \times n_2 \times n_3}$, resulting in $\hat{\mathcal{W}} = \text{fft}(\tilde{\mathcal{W}}, [], 3)$. For the transformed tensor $\hat{\mathcal{W}}$, we define the *column score* α_j to quantify the importance of column j , i.e.,

$$\alpha_j = \frac{\sum_{k=1}^{n_3} \|\hat{\mathcal{W}}(:, j, k)\|_2}{\sum_{j=1}^{n_2} \sum_{k=1}^{n_3} \|\hat{\mathcal{W}}(:, j, k)\|_2}, j = 1, 2, \dots, n_2, \quad (3)$$

where $\|\cdot\|_2$ denotes the 2-norm of the vector. The r column indices with the largest α_j values are

selected to form the set of column indices J . Similarly, the *row score* β_i is defined to quantify the importance of row i , i.e.,

$$\beta_i = \frac{\sum_{k=1}^{n_3} \|\widehat{\mathcal{W}}(i, J, k)\|_2}{\sum_{i=1}^{n_1} \sum_{k=1}^{n_3} \|\widehat{\mathcal{W}}(i, J, k)\|_2}, i = 1, 2, \dots, n_1. \quad (4)$$

The r row indices with the largest β_i values are selected to form the set of row indices I . Using the column index set J and the row index set I , we obtain:

$$\hat{\mathcal{C}} = \widehat{\mathcal{W}}(:, J, :), \hat{\mathcal{U}} = \widehat{\mathcal{W}}(I, J, :), \hat{\mathcal{R}} = \widehat{\mathcal{W}}(I, :, :).$$

Finally, we apply the inverse FFT to obtain the tensors \mathcal{C} , \mathcal{U} and \mathcal{R} :

$$\mathcal{C} = \text{ifft}(\hat{\mathcal{C}}, [], 3), \mathcal{U} = \text{ifft}(\hat{\mathcal{U}}, [], 3), \mathcal{R} = \text{ifft}(\hat{\mathcal{R}}, [], 3),$$

such that $\widetilde{\mathcal{W}} \approx \mathcal{C} * \mathcal{U}^\dagger * \mathcal{R}$.

The tensors \mathcal{C} and \mathcal{R} remain fixed throughout the fine-tuning process. To ensure the fine-tuning starts from the pre-trained parameter values, the tensor \mathcal{U} is initialized as a zero tensor and is continuously updated during the process.

2.3 tCURLoRA for Fine-Tuning UNETR Parameters

We now use our proposed tCURLoRA to fine-tune a specific neural network, i.e., the UNETR network [49], as an example. The UNETR network consists of an encoder and a decoder. The encoder is composed of 12 stacked Transformer layers, while the decoder includes convolutional layers, batch normalization, and ReLU activation functions. The encoder and decoder are connected through deconvolution, convolution, batch normalization, and ReLU. For a detailed description of the UNETR architecture, please refer to [49]. Since most of the parameters in UNETR are concentrated in the Transformer modules, the proposed tCURLoRA method specifically fine-tunes the Transformer parameters while updating those of the decoder. Meanwhile, the parameters in the skip connections remain frozen.

The Transformer architecture primarily consists of two modules: the Multi-Head Self-Attention (MHSA) and the Multi-Layer Perceptron (MLP). In the MHSA module, the computation of queries, keys, values, and outputs is parameterized by matrices $W_q, W_k, W_v, W_o \in R^{d \times d}$. These matrices are divided into N_h heads, with each head corresponding to different matrices $W_q^{(i)}, W_k^{(i)}, W_v^{(i)}, W_o^{(i)} \in R^{d \times d_h}, i = 1, 2, \dots, N_h, d_h = d/N_h$. The computation in the MHSA module can be expressed as:

$$\text{MHSA}(X) = \sum_{i=1}^{N_h} \text{softmax}\left(\frac{XW_q^{(i)}W_k^{(i)T}X^T}{\sqrt{d_h}}\right)XW_v^{(i)}W_o^{(i)T}.$$

The MLP module consists of two fully connected layers. Ignoring the bias terms, the computation in this module can be expressed as:

$$\text{MLP}(X) = \text{GELU}(XW_{up})W_{down},$$

where GELU is the Gaussian Error Linear Unit activation function [51], and $W_{up} \in R^{d \times 4d}$ and $W_{down} \in R^{4d \times d}$ are the weight matrices for the first and second layers, respectively.

According to the above definitions, each Transformer layer contains four $d \times d$ matrices from the MHSA module, as well as one $d \times 4d$ matrix and one $4d \times d$ matrix from the MLP module.

Therefore, the UNETR network contains a total of 48 $d \times d$ matrices, 12 $d \times 4d$ matrices, and 12 $4d \times d$ matrices. To organize these matrices, we concatenate them along the frontal dimension to form three tensors: $\mathcal{W}_{sa} \in R^{d \times d \times 48}$, $\mathcal{W}_{up} \in R^{d \times 4d \times 12}$ and $\mathcal{W}_{down} \in R^{4d \times d \times 12}$. In the tCURLoRA method, these three tensors are fine-tuned separately to efficiently optimize the model’s performance.

For completion, we summarize our tCURLoRA method in Algorithm 1.

Algorithm 1. tCURLoRA for Fine-Tuning

Input: Tensor $\tilde{\mathcal{W}} \in R^{n_1 \times n_2 \times n_3}$; sample size r .

1. Initialization:

- (a) Initialize the tensor \mathcal{U} as a zero tensor.
- (b) Compute the Fourier transform of $\tilde{\mathcal{W}}$: $\hat{\mathcal{W}} = \text{fft}(\tilde{\mathcal{W}}, [], 3)$.
- (c) Calculate the column scores α_j and row scores β_i using Equations (3) and (4), respectively. Select the r largest α_j and β_i values to form the sets of column indices J and row indices I .
- (d) Extract the corresponding columns and rows of $\hat{\mathcal{W}}$: $\hat{\mathcal{C}} = \hat{\mathcal{W}}(:, J, :)$, $\hat{\mathcal{R}} = \hat{\mathcal{W}}(I, :, :)$. Compute the inverse Fourier transform to obtain $\mathcal{C} = \text{ifft}(\hat{\mathcal{C}}, [], 3)$ and $\mathcal{R} = \text{ifft}(\hat{\mathcal{R}}, [], 3)$.

2. Fine-Tuning:

During fine-tuning, $\tilde{\mathcal{W}}$ remains fixed, while only the tensor increment $\Delta\mathcal{W} = \mathcal{C} * \mathcal{U} * \mathcal{R}$ is updated. The gradient flows through $\Delta\mathcal{W}$, which is updated via \mathcal{U} , as \mathcal{C} and \mathcal{R} are fixed.

4. Experiments and Results

4.1 Dataset

4.1.1 Dataset for Pre-training

The UNETR model is first pre-trained on the BraTS2021 dataset [52], which is a key resource in the field of brain tumor segmentation. The dataset includes multimodal magnetic resonance imaging (MRI) data, specifically T1, T1ce, T2, and FLAIR imaging modalities. For each patient, the imaging data has a resolution of $240 \times 240 \times 155$ with a voxel size of $1 \times 1 \times 1 \text{mm}^3$. The dataset provides detailed tumor region annotations for 1,251 cases, categorized into three regions: enhancing tumor (ET), peritumoral edema/infiltrative tissue (ED), and necrotic tumor core (NCR).

4.1.2 Datasets for Downstream Tasks

We apply the tCURLoRA method to transfer the pre-trained UNETR segmentation model to three downstream task datasets, including the EADC-ADNI dataset [53], the LPBA40 dataset [54], and the UPENN-GBM dataset [55].

The EADC-ADNI dataset is based on the ADNI database (<http://adni.loni.usc.edu/>) and contains MRI scan data from 135 patients, with an image resolution of $197 \times 233 \times 189$ and a voxel size of $1 \times 1 \times 1 \text{mm}^3$. The ADNI was launched in 2003 as a public-private partnership. Its initial objective was to assess whether combining serial MRI, positron emission tomography (PET), other biomarkers, and clinical and neuropsychological assessments could effectively track the progression of mild cognitive impairment (MCI) and early Alzheimer’s disease (AD). Currently, ADNI aims to validate biomarkers for clinical trials, enhance data generalizability by increasing participant diversity, and provide insights into the diagnosis and progression of Alzheimer’s disease. For the latest information, visit adni.loni.usc.edu.

The hippocampal region annotations for each image adhere to the harmonized segmentation protocol proposed by the European Alzheimer’s Disease Consortium and the Alzheimer’s Disease Neuroimaging Initiative [53], available at www.hippocampal-protocol.net. During data quality inspection, we identified mismatches between the hippocampal annotations and imaging data for 5 patients. These cases were excluded to ensure the accuracy of the dataset and annotations.

The LPBA40 dataset, developed by the Laboratory of Neuroimaging (LONI), is a widely used and important resource in neuroimaging research [54]. This dataset provides 3D brain MRI scans from 40 healthy adults, with an image resolution of $256 \times 124 \times 256$ and voxel dimensions of $0.8938 \times 1.500 \times 0.8594$ mm³. All scans are accompanied by detailed manual annotations, covering 56 types of brain tissues and anatomical structures. In this study, we selected the hippocampal region annotation data from this dataset to validate the effectiveness of the proposed method.

The UPENN-GBM dataset includes MRI data from 630 glioblastoma patients at the University of Pennsylvania Health System, encompassing imaging, clinical, and radiomics information. The data is available through the Cancer Imaging Archive (TCIA) hosted by the National Cancer Institute [55]. All MRI scans were acquired pre-operatively using a 3T MRI scanner, with imaging modalities including T1, T2, contrast-enhanced T1 (T1GD), FLAIR, and corresponding segmentation labels. In this dataset, MRI scans from 147 patients were annotated by clinical experts, with key sub-regions such as necrotic core (NC), peritumoral edema (ED), and enhancing tumor (ET) clearly identified. This study uses the 147 expert-annotated images, selecting T1GD modality images and defining the Whole Tumor (WT) region as the segmentation target, which encompasses all parts of the brain tumor.

All images in the datasets mentioned above underwent skull stripping and were registered to the MNI152 standard space, resulting in a processed voxel size of $1 \times 1 \times 1$ mm³.

4.2 Evaluation Metrics

We use the Dice coefficient and the 95th percentile Hausdorff distance (HD95) as evaluation metrics for segmentation performance. The Dice coefficient measures the volume overlap between the automated segmentation and the ground truth, and is calculated as:

$$Dice = 2 \frac{V(A \cap B)}{V(A) + V(B)},$$

where A represents the ground truth, B represents the automated segmentation, and $V(S)$ denotes the volume of set S . HD95 is a more robust version of the Hausdorff distance, used to quantify boundary consistency of the segmentation results. It is defined as:

$$HD95(A, B) = \max(h_{95}(A, B), h_{95}(B, A)),$$

where $h_{95}(A, B) = K_{a \in A}^{95} \min_{b \in B} d(a, b)$ represents the 95th percentile of the minimum Euclidean distance from boundary points in set A to boundary points in set B . This metric effectively evaluates the boundary robustness and accuracy of the segmentation results.

4.3 Experimental Details

We conducted experiments using the PyTorch framework, with two NVIDIA GeForce RTX 4090D GPUs. In the pre-training phase, we combined the three annotated regions from the BraTS2021 dataset into a single tumor region as the target for segmentation. The network was trained using only T1ce

modality data. The 1,251 publicly annotated samples were divided into training, validation, and test sets with a ratio of 8:1:1, resulting in 1,000 samples for training, 125 for validation, and 126 for testing. Hyperparameter settings during training followed the original configuration from the UNETR paper [49].

In the fine-tuning phase, for the EADC-ADNI and LPBA40 datasets, we randomly selected 5 samples for training, reserving the rest for testing. For the UPENN-GBM dataset, 10% of the samples were randomly chosen for training, with the remaining used for testing. During training, we employed the Adam optimizer with a batch size of 4 and applied polynomial learning rate decay. The initial learning rate was set to 0.001, decaying by a factor of 0.9 at each iteration. Image inputs were randomly cropped into $128 \times 128 \times 128$ patches, with the following augmentation strategies: (1) random mirroring along the axial, coronal, and sagittal planes with a 50% probability; (2) random intensity shifts within the range of $[-0.1, 0.1]$ for each pixel; and (3) random scaling within the range of $[0.9, 1.1]$. The loss function used by the network was the Dice loss, defined as:

$$\mathcal{L}(Y, \tilde{Y}) = -\frac{1}{N} \sum_{n=1}^N \frac{2Y_n \tilde{Y}_n}{Y_n + \tilde{Y}_n},$$

where Y_n and \tilde{Y}_n represent the ground truth and predicted probabilities, respectively, and N is the batch size. The loss function also included L2 regularization with a weight decay rate of 10^{-5} . Training was stopped after 1000 epochs.

During testing, we extracted $128 \times 128 \times 128$ image patches and applied a non-overlapping sliding window strategy to input them into the trained model for segmentation. The final inference result was obtained by averaging the model outputs from the last four epochs. In the post-processing phase, we removed false-positive segmentation results by first creating a binary mask to identify all connected regions, using a threshold of 1000 voxels (i.e., 1 cm^3). Any region smaller than this threshold was discarded and labeled as background.

4.4 Experimental Results

We compared the proposed tCURLoRA method with existing PEFT methods, including Full fine-tuning (Full), Linear-probing (Linear), LoRA [5], Adapter[56], SSF[57], LoTR[45], PiSSA[7] and CURLoRA[8]. In detail, full fine-tuning updates all model parameters; linear probing only updates the parameters of the linear layers within the Transformer module; LoRA represents the weight matrix increment as the product of two low-rank matrices, updating only the parameters of these matrices during fine-tuning; Adapter optimizes the visual model via structural reparameterization to improve adaptability to new tasks while reducing computational complexity; SSF introduces scaling and rotation factors after each operation in the Transformer (such as multi-head attention, MLP, and LN), updating only the newly added parameters while keeping other parameters frozen; LoTR adjusts neural network weights using Tucker tensor decomposition for task adaptation; PiSSA achieves model transfer by adjusting the dominant singular values and singular vectors; and CURLoRA utilizes matrix CUR decomposition, updating only the U matrix in the fine-tuning phase.

Since the rank r is a critical hyperparameter influencing the performance of LoRA, Adapter, LoTR, PiSSA, CURLoRA, and the proposed tCURLoRA method, we first assessed these methods' performance with different rank values on the EADC-ADNI dataset. Table 1 shows the Dice scores for segmentation results across various rank settings. The results indicate that the optimal rank for LoRA and Adapter is

$r=32$, for LoTR, PiSSA, and CURLoRA it is $r=2$, and for tCURLoRA it is $r=8$. It is worth highlighting that: i) our method, tCURLoRA is actually quite robust regarding different rank r , showing only a 0.14 accuracy difference compared to other methods like LoRA, which results in an accuracy difference greater than 0.5; and ii) tCURLoRA is very effective, i.e., its lowest accuracy 84.81 is already better than the best accuracy of all other methods, which is 84.64. In the following experiments, unless otherwise specified, we used these optimal rank values.

Table 1. Dice scores for segmentation results of different fine-tuning methods at various rank values r on the EADC-ADNI dataset, with the best results highlighted in **bold**.

Method	$r=1$	$r=2$	$r=4$	$r=8$	$r=16$	$r=32$
LoRA	84.28	84.00	83.64	84.06	84.10	84.35
Adapter	83.58	83.80	83.91	83.49	83.74	84.08
LoTR	83.83	84.05	83.85	83.63	83.67	83.50
PISSA	84.16	84.25	83.91	83.68	83.91	83.86
CURLoRA	84.62	84.64	84.63	84.60	84.62	84.57
tCURLoRA	84.88	84.89	84.81	84.95	84.88	84.86

Table 2. Comparison of segmentation results of different fine-tuning methods on three datasets, in terms of Dice and HD95 metrics. The best results are highlighted in **bold**.

Method	Params (M)	EADC-ADNI		LPBA40		UPENN-GBM	
		Dice	HD95	Dice	HD95	Dice	HD95
Full	90.011	83.79	5.839	79.91	7.175	69.95	32.280
Linear	59.348	83.46	5.344	80.62	6.483	72.42	29.401
LoRA	7.397	84.35	5.334	80.17	6.618	72.51	29.799
Adapter	7.987	84.08	5.663	79.72	6.793	73.46	33.357
SSF	2.883	83.73	5.326	79.08	6.904	72.29	28.762
LoTR	2.703	84.05	5.394	80.21	7.011	71.14	32.093
PISSA	2.974	84.25	5.603	80.52	6.584	72.52	31.331
CURLoRA	2.679	84.64	5.549	79.96	6.659	72.73	29.387
tCURLoRA	2.683	84.95	4.855	81.12	6.305	74.28	30.550

Table 2 presents the segmentation performance of different methods across three datasets, i.e., EADC-ADNI, LPBA40, and UPENN-GBM. The proposed tCURLoRA method has a parameter count of 2.683M, which is comparable to SSF, LoTR, PISSA, and CURLoRA, and only 2.98% of the parameters in the full fine-tuning method. This substantial reduction in the number of trainable parameters leads to significant improvements in training efficiency. Despite this reduction, tCURLoRA maintains superior segmentation accuracy. Compared to full fine-tuning, which serves as the baseline, tCURLoRA improves the Dice coefficient by 1.16%, 1.21%, and 4.33% on the EADC-ADNI, LPBA40, and UPENN-GBM datasets, respectively. Simultaneously, the HD95 metric decreases by 0.984 (16.85%), 0.870 (12.13%), and 1.73 (5.36%), demonstrating superior segmentation precision and better capturing of local details. Additionally, tCURLoRA achieves the highest Dice coefficient compared to all other methods across three datasets, further validating its outstanding performance in segmentation accuracy. With the exception of the UPENN-GBM dataset, tCURLoRA also delivers the best results in HD95, highlighting its exceptional ability to maintain boundary accuracy and spatial precision.

Figure 2 presents the distribution of Dice coefficient and HD95 scores using box plots, providing a clear and visual comparison that underscores tCURLoRA’s consistently superior performance across multiple datasets. Figure 3 shows the actual segmentation results, including 2D slices and 3D surface visualizations. It is evident that tCURLoRA’s segmentation results closely align with the ground truth,

particularly when dealing with complex anatomical structures. The method excels in preserving fine details and reducing segmentation errors. These results further reinforce the effectiveness of tCURLoRA in medical image segmentation, demonstrating its ability to achieve high-quality results while maintaining training efficiency.

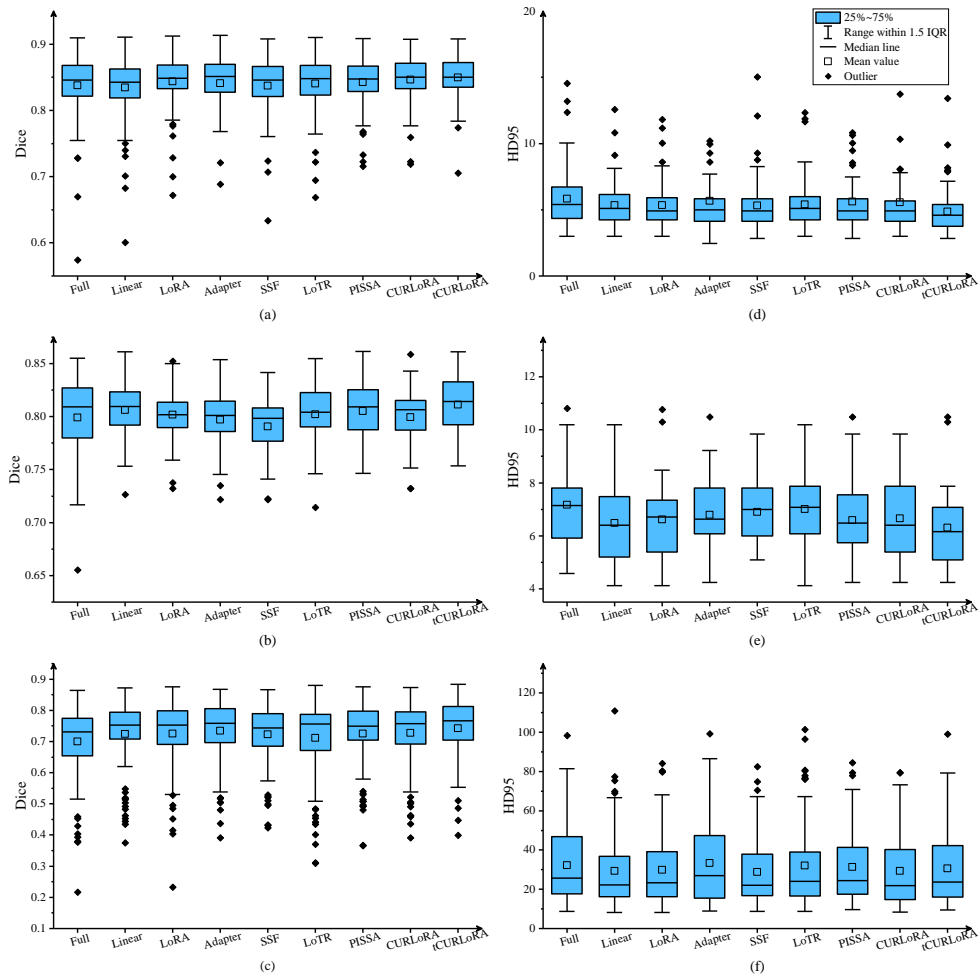


Figure 2. Box plots illustrating the segmentation performance in terms of Dice and HD95 metrics. (a) and (d) show the results for the Dice and HD95 scores on the EADC-ADNI dataset, respectively; (b) and (e) show the results on the LPBA40 dataset; and (c) and (f) show the results on the UPENN-GBM dataset.

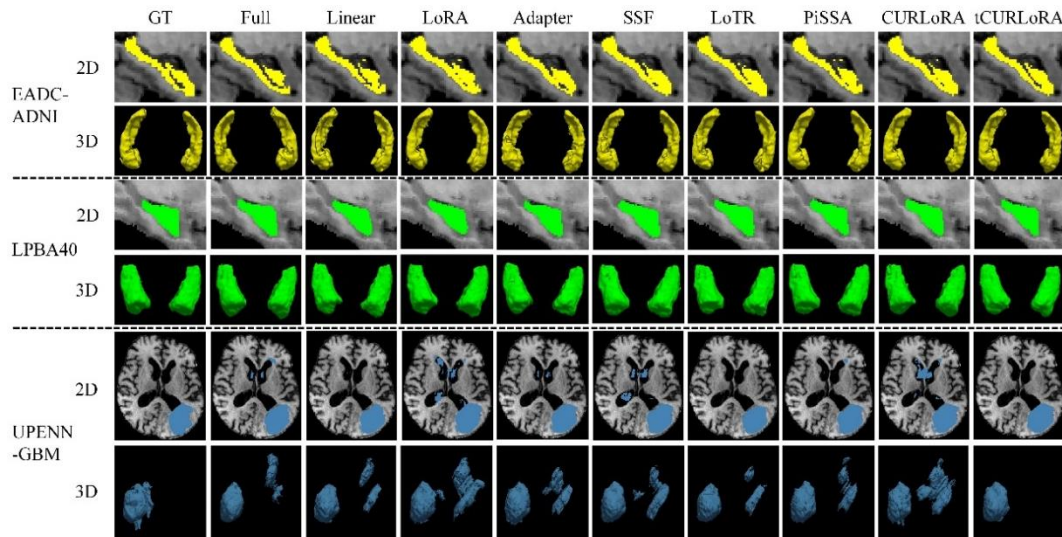


Figure 3. Qualitative segmentation results: 2D slices and 3D surfaces. Rows 1 and 2 display the segmentation results for a randomly selected subject from the EADC-ADNI dataset; rows 3 and 4 display the results for a randomly selected subject from the LPBA40 dataset; and rows 5 and 6 display the results for a randomly selected subject from the UPENN-GBM dataset.

5. Discussion and Conclusions

In this study, we proposed tCURLoRA, a tensor CUR decomposition-based fine-tuning method designed to enhance the efficiency of DNNs, and thoroughly studied an application in medical image segmentation tasks. By transforming pre-trained weight matrices into three-dimensional tensors and leveraging tensor CUR decomposition constraints during the fine-tuning process, tCURLoRA dramatically reduces the number of parameters requiring updates. This reduction not only lowers computational complexity and storage demands but also decreases the reliance on large datasets, making it particularly suitable for resource-constrained environments. Compared to traditional full fine-tuning methods, tCURLoRA offers significant improvements in parameter efficiency while maintaining high performance. The experimental results demonstrate that tCURLoRA consistently outperforms existing PEFT methods across multiple widely-used medical image segmentation datasets.

The incorporation of tensor CUR decomposition enables the better capture of higher-order relationships and multi-dimensional interactions within neural network weights, significantly enhancing the model’s representational power for complex tasks. Specifically, neural network weight matrices can be viewed as high-dimensional tensors that encode information across multiple dimensions, such as feature interactions at various levels. Traditional matrix factorization methods, such as LoRA, decompose the weight matrix into low-rank approximations of its row and column spaces, thereby reducing the number of parameters to be updated. While effective in reducing computational and storage overhead, these methods fail to capture the higher-order structures and complex interactions between dimensions inherent in the weight matrix. In contrast, tensor CUR decomposition transforms the weight matrix into a three-dimensional tensor, offering a richer, more comprehensive representation of these multi-dimensional interactions. This approach enhances the flexibility and expressiveness of the fine-tuning process, leading to improved performance in medical image segmentation tasks.

In comparison to the matrix-based CURLoRA method, tCURLoRA demonstrates superior expressive power in high-dimensional data scenarios. The matrix-based CURLoRA method fine-tunes by independently decomposing the weight matrices of each layer. However, this approach fails to effectively capture the nonlinear relationships between layers, which can lead to performance bottlenecks, particularly in complex tasks. In contrast, tCURLoRA leverages a higher-dimensional tensor representation, enabling the model to capture intricate multi-level interactions. This significantly enhances the model’s ability to process and learn from high-dimensional data, resulting in a notable performance improvement. Experimental results confirm this advantage, with tCURLoRA consistently outperforming the matrix-based CURLoRA method in terms of both the Dice coefficient and the HD95 metric across multiple datasets, underscoring the distinct benefits of tensor decomposition for efficient fine-tuning.

In conclusion, tCURLoRA offers an innovative and efficient fine-tuning approach. By reducing the number of learnable parameters and controlling computational complexity, tCURLoRA effectively addresses challenges related to training data, storage, and computation in large-scale deep learning applications, while achieving superior accuracy. Future research could explore its application in a broader

range of tasks and datasets, particularly in multimodal data processing and large-scale image segmentation. Further optimization of tCURLoRA's performance could also enhance its adaptability to real-world applications, making it a powerful tool for meeting the evolving demands across diverse fields.

Declaration of competing interest

The authors declare no financial interests or personal relationships that could have influenced this work.

Acknowledgments

Gaohang Yu's work was supported in part by National Natural Science Foundation of China (No. 12071104) and Guanghua He's work was supported by Scientific Research Project of Shaoxing University (No. 20210038).

Data collection and sharing for the Alzheimer's Disease Neuroimaging Initiative (ADNI) is funded by the National Institute on Aging (National Institutes of Health Grant U19AG024904). The grantee organization is the Northern California Institute for Research and Education. In the past, ADNI has also received funding from the National Institute of Biomedical Imaging and Bioengineering, the Canadian Institutes of Health Research, and private sector contributions through the Foundation for the National Institutes of Health (FNIH) including generous contributions from the following: AbbVie, Alzheimer's Association; Alzheimer's Drug Discovery Foundation; Araclon Biotech; BioClinica, Inc.; Biogen; BristolMyers Squibb Company; CereSpir, Inc.; Cogstate; Eisai Inc.; Elan Pharmaceuticals, Inc.; Eli Lilly and Company; EuroImmun; F. Hoffmann-La Roche Ltd and its affiliated company Genentech, Inc.; Fujirebio; GE Healthcare; IXICO Ltd.; Janssen Alzheimer Immunotherapy Research & Development, LLC.; Johnson & Johnson Pharmaceutical Research & Development LLC.; Lumosity; Lundbeck; Merck & Co., Inc.; Meso Scale Diagnostics, LLC.; NeuroRx Research; Neurotrack Technologies; Novartis Pharmaceuticals Corporation; Pfizer Inc.; Piramal Imaging; Servier; Takeda Pharmaceutical Company; and Transition Therapeutics.

References

- [1] S.J. Pan, Q. Yang, A survey on transfer learning, *IEEE Transactions on knowledge data engineering*, 22 (2009) 1345-1359.
- [2] K. Weiss, T.M. Khoshgoftaar, D. Wang, A survey of transfer learning, *Journal of Big data*, 3 (2016) 1-40.
- [3] N. Ding, Y. Qin, G. Yang, F. Wei, Z. Yang, Y. Su, S. Hu, Y. Chen, C.-M. Chan, W. Chen, Parameter-efficient fine-tuning of large-scale pre-trained language models, *Nature Machine Intelligence*, 5 (2023) 220-235.
- [4] Z. Han, C. Gao, J. Liu, J. Zhang, S.Q. Zhang, Parameter-efficient fine-tuning for large models: A comprehensive survey, *arXiv preprint arXiv:14608*, (2024).
- [5] E.J. Hu, Y. Shen, P. Wallis, Z. Allen-Zhu, Y. Li, S. Wang, L. Wang, W. Chen, Lora: Low-rank adaptation of large language models, *arXiv preprint arXiv:09685*, (2021).
- [6] S. Kim, H. Yang, Y. Kim, Y. Hong, E. Park, Hydra: Multi-head low-rank adaptation for parameter efficient fine-tuning, *Neural Networks*, (2024) 106414.
- [7] F. Meng, Z. Wang, M. Zhang, Pissa: Principal singular values and singular vectors adaptation of large language models, *arXiv preprint arXiv:2404.02948*, (2024).
- [8] M. Fawi, CURLoRA: Stable LLM Continual Fine-Tuning and Catastrophic Forgetting Mitigation, *arXiv preprint arXiv:2408.14572*, (2024).
- [9] Q. Wang, X. Hu, W. Xu, W. Liu, J. Luan, B. Wang, PMSS: Pretrained Matrices Skeleton Selection for LLM Fine-tuning, *arXiv preprint arXiv:2409.16722*, (2024).

- [10] Y. Panagakis, J. Kossaifi, G.G. Chrysos, J. Oldfield, M.A. Nicolaou, A. Anandkumar, S. Zafeiriou, Tensor methods in computer vision and deep learning, *Proceedings of the IEEE*, 109 (2021) 863-890.
- [11] Y. LeCun, L. Bottou, Y. Bengio, P. Haffner, Gradient-based learning applied to document recognition, *Proceedings of the IEEE*, 86 (1998) 2278-2324.
- [12] A. Krizhevsky, I. Sutskever, G.E. Hinton, Imagenet classification with deep convolutional neural networks, *Advances in neural information processing systems*, 25 (2012).
- [13] K. Simonyan, A. Zisserman, Very deep convolutional networks for large-scale image recognition, *arXiv preprint arXiv:1409.1556*, (2014).
- [14] K. He, X. Zhang, S. Ren, J. Sun, Deep residual learning for image recognition, *Proceedings of the IEEE conference on computer vision and pattern recognition2016*, pp. 770-778.
- [15] A. Vaswani, Attention is all you need, *Advances in Neural Information Processing Systems*, (2017).
- [16] J. Long, E. Shelhamer, T. Darrell, Fully convolutional networks for semantic segmentation, *Proceedings of the IEEE conference on computer vision and pattern recognition2015*, pp. 3431-3440.
- [17] O. Ronneberger, P. Fischer, T. Brox, U-net: Convolutional networks for biomedical image segmentation, *Medical image computing and computer-assisted intervention–MICCAI 2015: 18th international conference, Munich, Germany, October 5-9, 2015, proceedings, part III 18*, (Springer2015), pp. 234-241.
- [18] L.-C. Chen, G. Papandreou, I. Kokkinos, K. Murphy, A.L. Yuille, Deeplab: Semantic image segmentation with deep convolutional nets, atrous convolution, and fully connected crfs, *IEEE transactions on pattern analysis and machine intelligence*, 40 (2017) 834-848.
- [19] K. He, G. Gkioxari, P. Dollár, R. Girshick, Mask r-cnn, *Proceedings of the IEEE international conference on computer vision2017*, pp. 2961-2969.
- [20] L.-C. Chen, Y. Zhu, G. Papandreou, F. Schroff, H. Adam, Encoder-decoder with atrous separable convolution for semantic image segmentation, *Proceedings of the European conference on computer vision (ECCV)2018*, pp. 801-818.
- [21] A. Dosovitskiy, An image is worth 16x16 words: Transformers for image recognition at scale, *arXiv preprint arXiv:2010.11929*, (2020).
- [22] T.G. Kolda, B.W. Bader, Tensor decompositions and applications, *SIAM review*, 51 (2009) 455-500.
- [23] Y. Liu, J. Liu, Z. Long, C. Zhu, *Tensor computation for data analysis* (Springer, 2022).
- [24] H.A. Kiers, Towards a standardized notation and terminology in multiway analysis, *Journal of Chemometrics: A Journal of the Chemometrics Society*, 14 (2000) 105-122.
- [25] J. Mocks, Topographic components model for event-related potentials and some biophysical considerations, *IEEE transactions on biomedical engineering*, 35 (1988) 482-484.
- [26] L.R. Tucker, Some mathematical notes on three-mode factor analysis, *Psychometrika*, 31 (1966) 279-311.
- [27] I.V. Oseledets, Tensor-train decomposition, *SIAM Journal on Scientific Computing*, 33 (2011) 2295-2317.
- [28] M.W. Mahoney, M. Maggioni, P. Drineas, Tensor-CUR decompositions for tensor-based data, *Proceedings of the 12th ACM SIGKDD international conference on Knowledge discovery and data mining2006*, pp. 327-336.
- [29] J. Chen, Y. Wei, Y. Xu, Tensor CUR decomposition under T-product and its perturbation, *Numerical Functional Analysis and Optimization*, 43 (2022) 698-722.
- [30] C. Battaglino, G. Ballard, T.G. Kolda, A practical randomized CP tensor decomposition, *SIAM Journal on Matrix Analysis and Applications*, 39 (2018) 876-901.
- [31] M. Che, Y. Wei, H. Yan, An efficient randomized algorithm for computing the approximate Tucker decomposition, *Journal of Scientific Computing*, 88 (2021) 32.
- [32] W. Dong, G. Yu, L. Qi, X. Cai, Practical sketching algorithms for low-rank Tucker approximation of large tensors, *Journal of Scientific Computing*, 95 (2023) 52.
- [33] G. Yu, J. Feng, Z. Chen, X. Cai, L. Qi, A randomized block Krylov method for tensor train approximation, *arXiv preprint arXiv:2308.01480*, (2023).
- [34] H. Cai, Z. Chao, L. Huang, D. Needell, Fast robust tensor principal component analysis via fiber CUR decomposition, *Proceedings of the IEEE/CVF International Conference on Computer Vision2021*, pp. 189-197.
- [35] D. Bacciu, D.P. Mandic, Tensor decompositions in deep learning, *arXiv preprint arXiv:2002.11835*, (2020).
- [36] A.-H. Phan, K. Sobolev, K. Sozykin, D. Ermilov, J. Gusak, P. Tichavský, V. Glukhov, I. Oseledets, A. Cichocki, Stable low-rank tensor decomposition for compression of convolutional neural

network, Computer Vision–ECCV 2020: 16th European Conference, Glasgow, UK, August 23–28, 2020, Proceedings, Part XXIX 16, (Springer2020), pp. 522-539.

[37] L. Liebenwein, A. Maalouf, D. Feldman, D. Rus, Compressing neural networks: Towards determining the optimal layer-wise decomposition, *Advances in Neural Information Processing Systems*, 34 (2021) 5328-5344.

[38] D. Wang, G. Zhao, G. Li, L. Deng, Y. Wu, Compressing 3DCNNs based on tensor train decomposition, *Neural Networks*, 131 (2020) 215-230.

[39] H. Ben-Younes, R. Cadene, M. Cord, N. Thome, Mutan: Multimodal tucker fusion for visual question answering, *Proceedings of the IEEE international conference on computer vision2017*), pp. 2612-2620.

[40] R. Zhang, Z. Wang, H. Sun, L. Deng, H. Zhu, TDFusion: When tensor decomposition meets medical image fusion in the nonsubsampling shearlet transform domain, *Sensors*, 23 (2023) 6616.

[41] Y. Liang, Z. Shi, Z. Song, Y. Zhou, Tensor attention training: Provably efficient learning of higher-order transformers, *arXiv preprint arXiv:2405.16411*, (2024).

[42] M. Yin, Y. Sui, S. Liao, B. Yuan, Towards efficient tensor decomposition-based dnn model compression with optimization framework, *Proceedings of the IEEE/CVF Conference on Computer Vision and Pattern Recognition2021*), pp. 10674-10683.

[43] X. Chen, J. Liu, Y. Wang, M. Brand, G. Wang, T. Koike-Akino, SuperLoRA: Parameter-Efficient Unified Adaptation of Multi-Layer Attention Modules, *arXiv preprint arXiv:2403.11887*, (2024).

[44] S.-Y. Liu, C.-Y. Wang, H. Yin, P. Molchanov, Y.-C.F. Wang, K.-T. Cheng, M.-H. Chen, Dora: Weight-decomposed low-rank adaptation, *arXiv preprint arXiv:09353*, (2024).

[45] D. Bershatsky, D. Cherniuk, T. Daulbaev, I. Oseledets, LoTR: Low tensor rank weight adaptation, *arXiv preprint arXiv:2402.01376*, (2024).

[46] S. Jie, Z.-H. Deng, Fact: Factor-tuning for lightweight adaptation on vision transformer, *Proceedings of the AAAI conference on artificial intelligence2023*), pp. 1060-1068.

[47] C. Si, X. Wang, X. Yang, Z. Xu, Q. Li, J. Dai, Y. Qiao, X. Yang, W. Shen, FLoRA: Low-Rank Core Space for N-dimension, *arXiv preprint arXiv:2405.14739*, (2024).

[48] G. He, W. Cheng, H. Zhu, G. Yu, LoRA-PT: Low-Rank Adapting UNETR for Hippocampus Segmentation Using Principal Tensor Singular Values and Vectors, *arXiv preprint arXiv:2407.11292*, (2024).

[49] A. Hatamizadeh, Y. Tang, V. Nath, D. Yang, A. Myronenko, B. Landman, H.R. Roth, D. Xu, Unetr: Transformers for 3d medical image segmentation, *Proceedings of the IEEE/CVF Winter Conference on Applications of Computer Vision*, (2022) 574-584.

[50] G.H. Golub, C.F. Van Loan, *Matrix computations* (JHU press, 2013).

[51] D. Hendrycks, K. Gimpel, Gaussian error linear units (gelus), *arXiv preprint arXiv:1606.08415*, (2016).

[52] U. Baid, S. Ghodasara, S. Mohan, M. Bilello, E. Calabrese, E. Colak, K. Farahani, J. Kalpathy-Cramer, F.C. Kitamura, S. Pati, The rsna-asnr-miccai brats 2021 benchmark on brain tumor segmentation and radiogenomic classification, *arXiv preprint arXiv:2107.02314*, (2021).

[53] M. Boccardi, M. Bocchetta, F.C. Morency, D.L. Collins, M. Nishikawa, R. Ganzola, M.J. Grothe, D. Wolf, A. Redolfi, M. Pievani, Training labels for hippocampal segmentation based on the EADC-ADNI harmonized hippocampal protocol, *Alzheimer's & Dementia*, 11 (2015) 175-183.

[54] D.W. Shattuck, M. Mirza, V. Adisetiyo, C. Hojatkashani, G. Salamon, K.L. Narr, R.A. Poldrack, R.M. Bilder, A.W.J.N. Toga, Construction of a 3D probabilistic atlas of human cortical structures, 39 (2008) 1064-1080.

[55] S. Bakas, C. Sako, H. Akbari, M. Bilello, A. Sotiras, G. Shukla, Multi-parametric magnetic resonance imaging (mpMRI) scans for de novo Glioblastoma (GBM) patients from the University of Pennsylvania Health System (UPENN-GBM), The Cancer Imaging Archive (TCIA) Public Access, (2021).

[56] G. Luo, M. Huang, Y. Zhou, X. Sun, G. Jiang, Z. Wang, R. Ji, Towards efficient visual adaptation via structural re-parameterization, *arXiv preprint arXiv:2302.08106*, (2023).

[57] D. Lian, D. Zhou, J. Feng, X. Wang, Scaling & shifting your features: A new baseline for efficient model tuning, *Advances in Neural Information Processing Systems*, 35 (2022) 109-123.